J. Fluid Mech. (1979), *vol.* 92, *part* 4, *pp.* 731–749
Printed in Great Britain

On the dispersion relation of random gravity waves. Part 2. An experiment

By HISASHI MITSUYASU, YI-YU KUO AND AKIRA MASUDA

Research Institute for Applied Mechanics,
Kyushu University, Fukuoka, Japan

(Received 5 July 1977)

Random waves are generated by wind in the first half of a wind-wave flume. The latter half of the flume is kept free from wind to measure the waves unaffected by the wind and wind-generated current. The random waves in the latter area are measured with a linear array of wave gauges, and their phase velocities and coherences are determined by a usual technique of the cross-spectral analysis. The measured results are compared with the nonlinear theory of two-dimensional random waves, which has been presented in part 1 of this paper (Masuda, Kuo & Mitsuyasu 1979). Agreement between the theory and the experiment is satisfactory, and observed characteristics of the phase velocity and coherence of the spectral components can be attributed to the effects of the nonlinearity and angular dispersion of the random waves.

1. Introduction

The linear theory of random waves, which assumes the wave field composed of an nfinite number of free waves of random phases, is a powerful tool for describing ocean waves. In the strict sense, however, the equations describing water waves are nonlinear, which introduces a number of interesting phenomena into the random wave field; generation of forced (bounded) waves (Tick 1959); the energy transfer among wave components (Phillips 1960; Hasselmann 1962); and phase velocity effects (Longuet-Higgins & Phillips 1962). In recent years much interest has been paid to the nonlinear dispersion relation in a random wave field (Ramamonjiarisoa 1974; Huang & Tung 1976, 1977; Weber & Barrik 1977; Barrik & Weber 1977). This is perhaps due to the increasing utilization of remote sensing techniques in ocean wave studies. The dispersion relation is needed to relate the spatial characteristics measured with remote sensors to the temporal characteristics measured by conventional methods.

This paper is concerned with the dispersion relation of wind waves. It should be mentioned, however, that the phase velocity of wind waves in the generation area is also affected by the wind and wind-generated current (Shemdin 1972; Kato 1974).

To sum up the problem, the phase velocity of the spectral component of the wind waves is affected by the following factors:

(1) nonlinearity of the wave motion;
(2) wind pressure exerted on the wave surface;
(3) drift current generated by the wind;
(4) angular dispersion of the spectral component.

0022-1120/79/4212-6640 $02.00

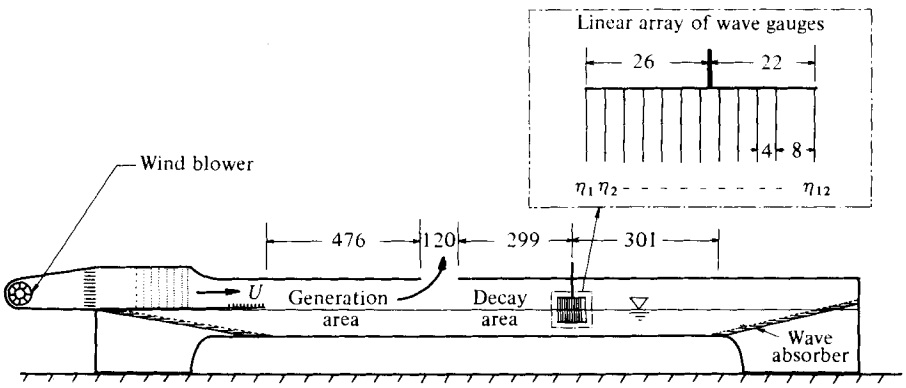

FIGURE 1. Schematic diagram of the wind-wave flume (units in cm).

More precisely, the nonlinearity of the wave motion influences the wave velocity in two ways: (i) to increase the phase velocity of the free waves in a similar way as in Stokes waves; and (ii) to generate the bounded secondary waves which propagate approximately twice as fast as the corresponding frequency component (free waves). In many cases, the effect of the wind pressure is much smaller than that of other factors. The influence of the drift current on the phase velocity may be very small for ocean waves, but it can be important for laboratory wind waves in the generation area because the wave velocity in the latter case is not so large as to make the current velocity negligible. Angular dispersion of the spectral component also influences the measured wave velocity in two ways: (i) the influence on the nonlinear interaction among spectral components (Masuda, Kuo & Mitsuyasu 1979) and (ii) the contributions to the cross-spectra, from which the wave velocity is determined (Yefimov, Solov'yev & Khristoforov 1972).

In order to study the effects of the nonlinearity and angular dispersion of waves on the phase velocities of spectral components, we have analysed the data of laboratory wind waves in the decay area where the wind and wind-generated current are absent. Measured results are compared with the nonlinear theory of two-dimensional random waves which has been presented in part 1 of this paper (Masuda *et al.* 1979; hereinafter referred to as I).

2. Equipment and procedure

Wind-wave flume

The measurements were made in a wind-wave flume 13·4 m long, 0·6 m wide and 0·8 m high. Water depth was kept 0·365 m throughout the experiment. Figure 1 shows the experimental arrangement. Wind waves were generated in the first half of the flume; the latter half of the flume was kept free from wind to measure the random wave field unaffected by the wind and drift current. The latter half of the flume was made airtight to eject the air flow smoothly from the ceiling gap at the middle part of the flume. It was confirmed that the drift current attenuates very rapidly in the decay area and is negligible at the location of the wave measurements.

Wave measurements

Waves were measured by using a linear array of twelve wave gauges aligned equidistantly with 4 cm intervals except for the last gauge (figure 1). Each probe of the wave gauge is of resistance-type, which consists of two parallel platinum wires with a diameter of 0·1 mm and 2 mm space. In the measurement of the wave velocity in the dominant direction of wave propagation, the linear array of the wave gauges was parallel to the longitudinal direction of the flume (figure 1). The linear array of wave gauges was also used for measuring the directional spectra of wind waves by changing the direction of the array (Cummins 1959). However, the details of the measurements of the directional wave spectra will be published in another paper, and only a part of the results will be used in the present analysis.

Experimental procedure

Winds with three different speeds $U = 10$, 12·5 and 15 m/s were used for generating wind waves with different spectral peak frequencies. Here U is a cross-sectional mean speed of the wind in the generation area of the flume. Wind-generated waves propagate from the generation area to the decay area in the latter half of the flume and are finally absorbed by the wave absorber installed at the end of the flume where the width of the flume is widened from 0·6 to 1 m. The reflexion of the waves was approximately below 3 %. In each run, waves were measured continuously for 13 min at the location shown in figure 1, and wave signals from twelve gauges were recorded on a FM data recorder.

3. Analysis of the wave data

The twelve wave records of each run were digitized simultaneously at a sampling frequency of 40 Hz. For the convenience of the spectral analysis, each of the wave data was divided into ten sub-samples of 51·2 s, which contained 2048 data points. In order to measure the phase velocity of the spectral components, cross-spectra

$$Cr(\omega, l) \equiv Co(\omega, l) - iQ(\omega, l) \tag{3.1}$$

were computed through the fast Fourier transform procedure, by using the first wave data η_1 nearest to the generation area and the succeeding wave data η_n ($n = 2, 3, \ldots, 12$). Here, ω is the angular frequency and l is the spacing between any two wave gauges.

In this way, we can compute the cross-spectra of waves measured at two points of different spacing ($l = 4, 8, 12, \ldots$ cm) along the dominant direction of wave propagation. Final data of the cross-spectra were obtained by taking sample mean of ten sub-samples of raw wave spectra and taking moving average of successive seven line spectra. Hence, equivalent degrees of freedom of the measured spectra are approximately 140. By using the cross-spectra of waves, the phase lag $\theta(\omega, l)$, the coherence coh (ω, l) and the phase velocity $C(\omega)$ of the spectral components were determined as

$$\theta(\omega, l) = \tan^{-1}[Q(\omega, l)/Co(\omega, l)], \tag{3.2}$$

$$\text{coh}\,(\omega, l) = \{[Co^2(\omega, l) + Q^2(\omega, l)]/\psi_{(1)}(\omega)\,\psi_{(n)}(\omega)\}^{\frac{1}{2}}, \quad n = 2, 3, \ldots, 12, \tag{3.3}$$

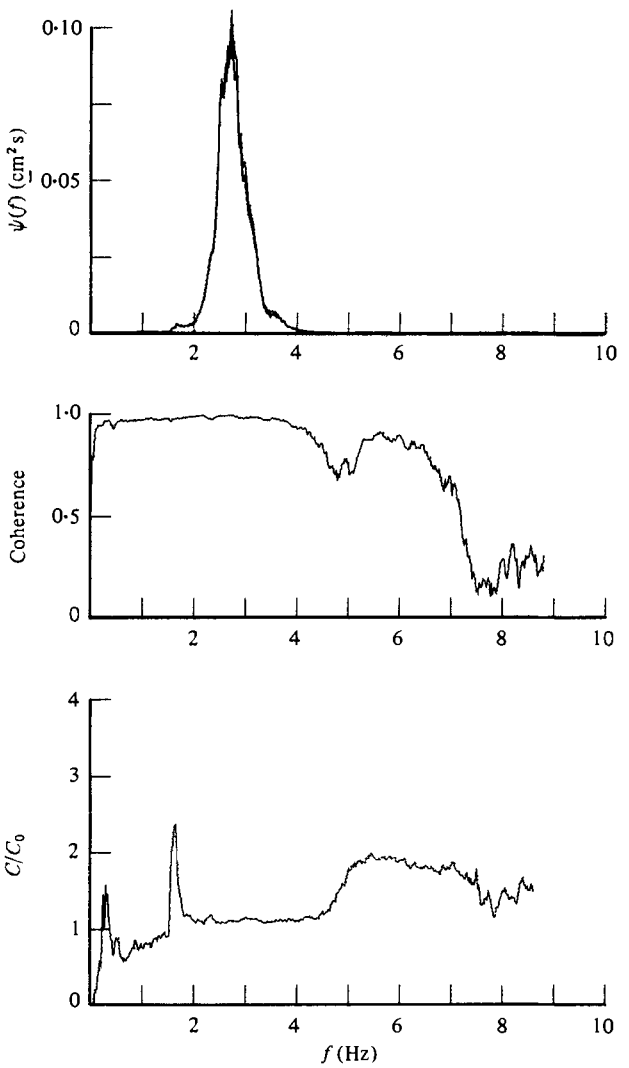

FIGURE 2. Power spectra and coherence of two wave records η_1 and η_2 ($l = 4$ cm), and normalized phase velocity of the spectral component for $U = 10$ m/s.

and
$$C(\omega) = \omega l/\theta(\omega, l), \tag{3.4}$$
where $\psi_{(1)}(\omega)$ and $\psi_{(n)}(\omega)$ are the frequency spectra of η_1 and η_n respectively.

4. Experimental results

Typical examples of the measured results are shown in figures 2–4. From the top to the bottom, power spectra at two stations, normalized phase velocity C/C_0 and coherence are shown respectively as a function of the frequency f. Here, C_0 is the phase velocity of long-crested linear waves in finite depth h, which is given by

$$C_0 = \frac{g}{\omega} \tanh \frac{2\pi h}{L}, \tag{4.1}$$

where g is the acceleration due to gravity and L is the wavelength.

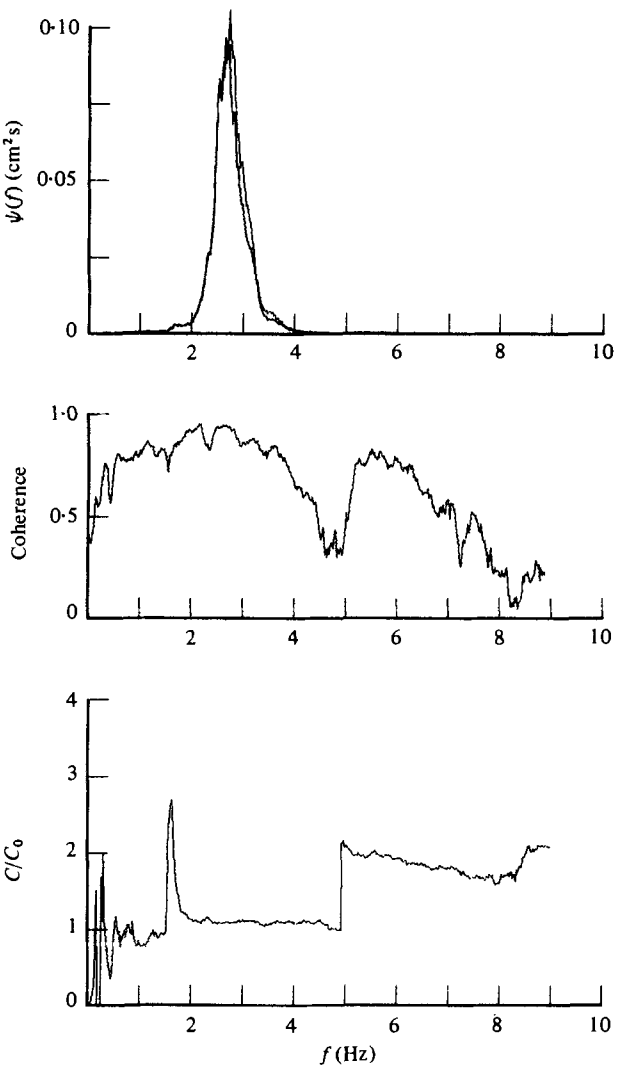

FIGURE 3. The same as figure 2 except for wave records η_1 and η_4 (l = 12 cm).

Power spectra

Since the attenuation of the spectral energy is very small for relatively short distance of propagation ($l \lesssim 12$ cm), power spectra at two stations almost coincide with each other. Spectral peak frequency f_m is 2·7 Hz for the waves generated by a wind with U = 10 m/s, and 1·8 Hz for those generated by a wind with U = 15 m/s. With the increase of the distance of wave propagation, attenuation of the wave energy ceases to be negligible. However, this problem will be discussed in another paper.

Coherence

The coherence of the waves measured at two stations are nearly unity for the frequency components near the spectral peak frequency f_m when the distance between two wave gauges is relatively short (l = 4, 12 cm). Although the data for very long distances are

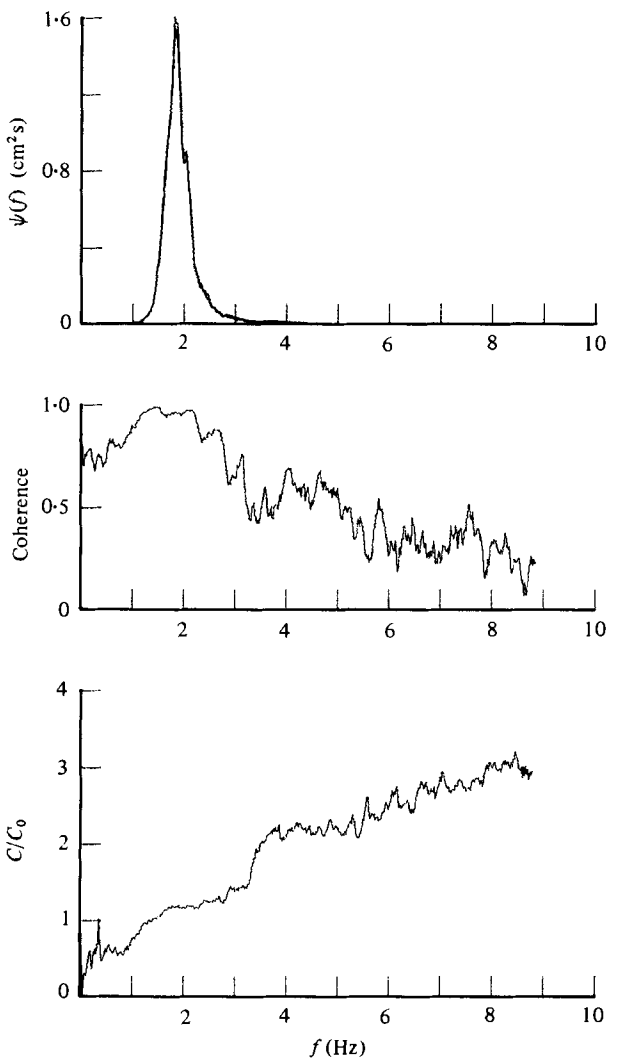

FIGURE 4. The same as figure 2 except for wave records η_1 and η_4 ($l = 12$ cm) and $U = 15$ m/s.

not shown in these figures the coherence near f_m decreases gradually with the increase of the distance between two wave gauges as will be shown later in figure 9. The coherence also decreases gradually with the increase of the frequency of the spectral component. In addition to such gradual decreases, very rapid decrease of the coherence can be seen locally near 4·8 and 8·5 Hz for $U = 10$ m/s, and near 3·4 Hz for $U = 15$ m/s. These frequencies of local drops of the coherence correspond roughly to twice or three times the spectral peak frequency f_m.

Phase velocity

The normalized phase velocity C/C_0 is nearly equal to but slightly larger than unity in a relatively wide frequency range near the spectral peak frequency. That is, the phase velocities of energy-containing components of random waves are fairly close to

those for the long-crested linear waves. It will be shown later that slight differences between C and C_0 can be attributed to the effect of angular spreading of random waves. However, the rapid increase of C/C_0 appears at the frequencies where the local decrease of the coherence is observed. Particularly, the increase of C/C_0 is very rapid for relatively large spacing of the wave gauges. These peculiar features of the coherence and phase velocity are attributed to the nonlinear effects of the random wave field which will be discussed later. Anomalous values of C/C_0 at 1·6 Hz, which are observed for $U = 10\,\mathrm{m/s}$, can be attributed to the transverse oscillation of water in the flume. Although the amplitude of the transverse oscillation is very small, it cannot be negligible when the spectral density of wind-generated waves is very small at that frequency. In fact, such phenomena are not seen for $U = 15\,\mathrm{m/s}$, because the spectral density of wind-generated waves has much larger values than those for $U = 10\,\mathrm{m/s}$ at that frequency.

5. Theoretical computations

In order to apply the nonlinear theory presented in I to the analysis of our measured waves, it is necessary to separate the measured spectrum $\Psi_{\mathrm{obs}}(\omega)$ into the spectrum of the free wave $\Psi_1(\omega)$ and that of the forced wave $\Psi_2(\omega)$:

$$\Psi_{\mathrm{obs}} = \Psi_1(\omega) + \Psi_2(\omega). \tag{5.1}$$

The separation can be done by the iterative method presented in I, where the angular distribution function $S(\omega, \theta)$ in equation (3.8) of I is assumed as

$$S(\omega,\theta) = \begin{cases} S'(m)\cos^m\theta & \text{for} \quad |\theta| \leqslant \tfrac{1}{2}\pi \\ 0 & \text{for} \quad |\theta| > \tfrac{1}{2}\pi, \end{cases} \tag{5.2}$$

where $S'(m)$ is a normalizing function.

Practical computations are summarized as follows: we assume $m = 2$, 4, 6 for the angular distribution function (5.2), compute $\Psi_1(\omega)$ and $\Psi_2(\omega)$ by the iterative method presented in I, and determine the cross spectrum $Cr(\omega, \mathbf{1})$ [$= Cr_1(\omega, \mathbf{1}) + Cr_2(\omega, \mathbf{1})$] by substituting $\Psi_1(\omega)$, $\Psi_2(\omega)$ and $S(\omega, \theta)$ into equation (2.30) of I. Finally, in order to compare the theory with the measurements, the coherence and the phase velocity are computed from (3.3) and (3.4) by using the cross spectrum. In the first order (linear) approximation, only $\Psi_1(\omega)$ and thus $Cr_1(\omega, \mathbf{1})$ are used in the above computations. In the third-order approximation we consider the nonlinear dispersion relation and use†

$$\delta(|\mathbf{k}| - \omega^2/g + \epsilon(\omega, \theta)), \tag{5.3}$$

instead of $\delta(|\mathbf{k}| - \omega^2/g)$, where $\epsilon(\omega, \theta)$ is an increment of $|\mathbf{k}|$ deduced by the nonlinear dispersion relation (2.23) of I.

Since the nonlinear effects for the phase velocity of deep-water waves is given by

$$\Delta C = C - C_0 = \omega/|\mathbf{k}| - g/\omega, \tag{5.4}$$

we can evaluate ΔC by computing the right-hand side of equation (2.24) of I. Several examples of the computed results are shown in figures 5 and 6, where the measured frequency spectrum is used for the computation and $S(\omega, \theta)$ is assumed as

$$S(\omega, \theta) \sim \cos^4\theta.$$

† It should be noted that g has been taken as unity in part 1 for convenience.

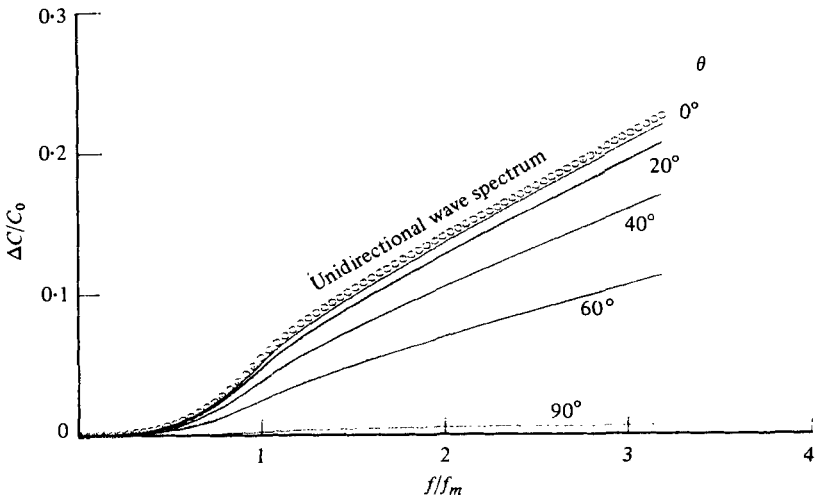

FIGURE 5. The change in the phase velocity of the spectral component $\Delta C/C_0$ *vs.* normalized frequency f/f_m for our measured wave spectrum ($U = 15$ m/s, wave η_1). ——, computed for the angular distribution function $S(\theta) \sim \cos^4\theta$; ○, computed for the unidirectional wave spectrum.

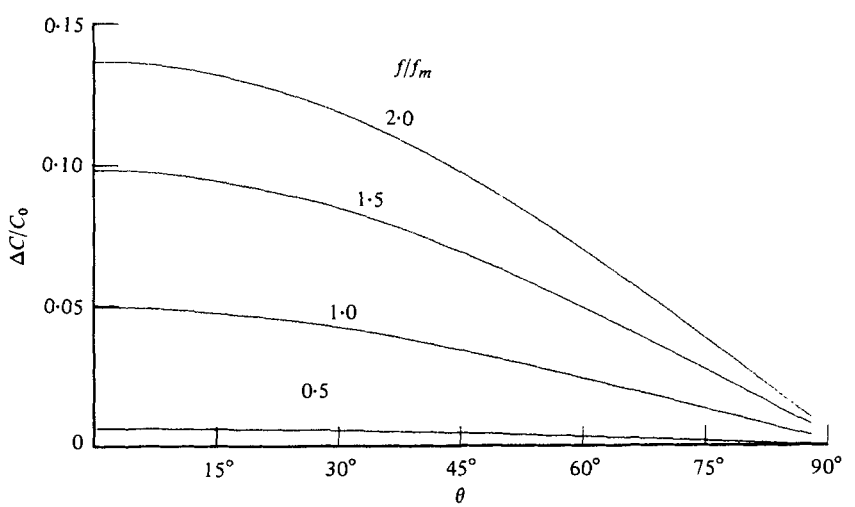

FIGURE 6. The change in phase velocity of the spectral component $\Delta C/C_0$ *vs.* θ the propagation direction for various f/f_m.

A more general representation is given in figure 7, which shows contours of $\Delta C/C_0$ normalized by the strength of nonlinearity $E_1(2\pi f_m)^4/g^2$ as a function of f/f_m and θ, where E_1 is the total energy of the free waves. A curve in the left-hand side of figure 7 shows the corresponding spectrum of the free wave $\Psi_1(f/f_m)$ in an arbitrary density scale which has been determined from the measured spectrum by the iterative method. From these figures we can evaluate the influence of the nonlinearity on the phase velocity of spectral components as a function of its relative frequency f/f_m and propagation direction θ. Figure 5 shows that the nonlinear effect on the phase velocity of free waves is at most 20% for the spectral components in a dominant part of our

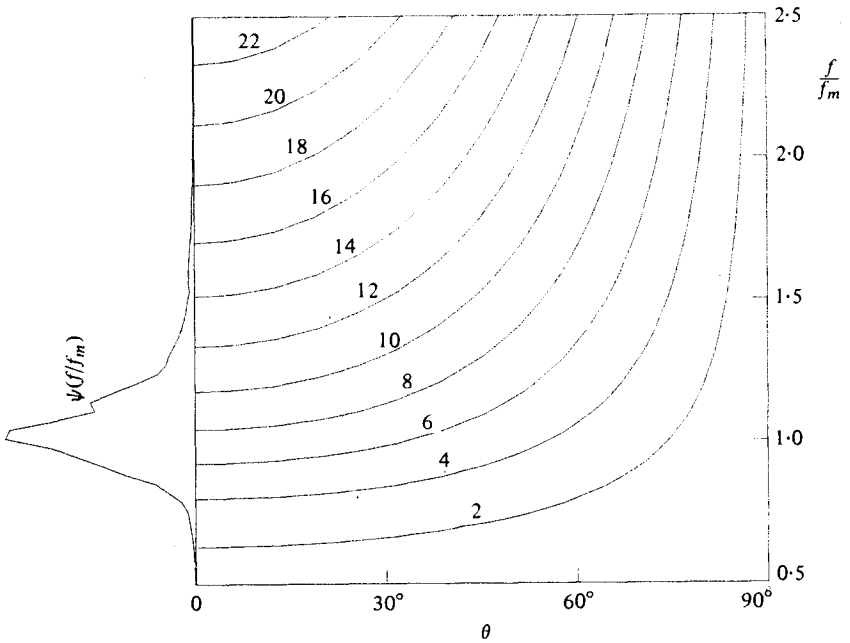

FIGURE 7. The same as figures 5 and 6 except that the contours of $\Delta C/C_0$ normalized by $E_1(2\pi f_m)^4/g^2$ are shown as a function of f/f_m and θ. The corresponding frequency spectrum ψ_1 is shown in the left-hand side with arbitrary density scale.

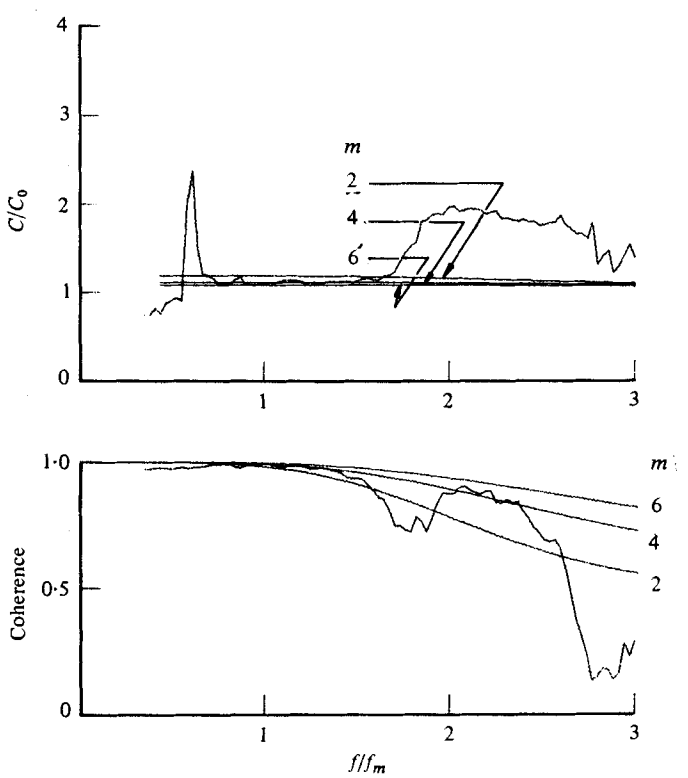

FIGURE 8. Comparison of the linear theory with the measured phase velocity and coherence for $U = 10\,\text{m/s}$ and $l = 4\,\text{cm}$. The angular distribution function is assumed as $S(\theta) \sim \cos^m \theta$, $m = 2, 4, 6$.

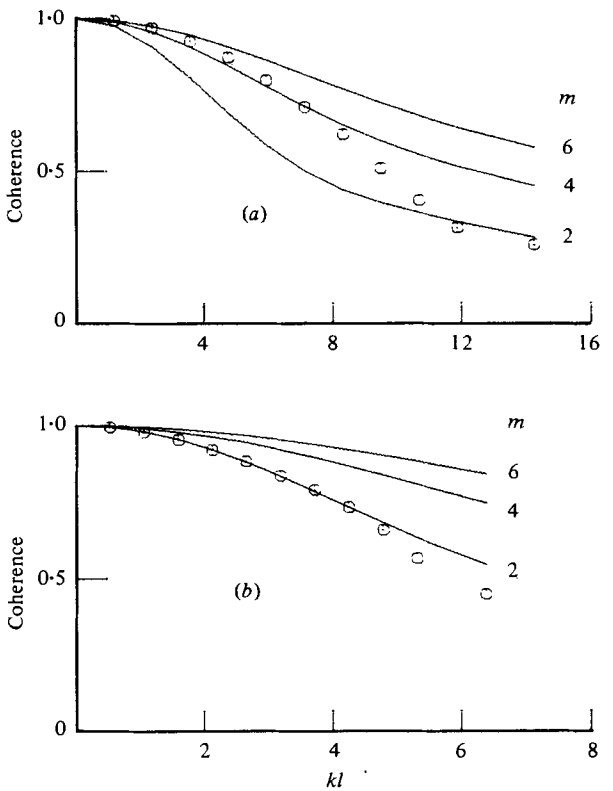

FIGURE 9. Comparison of the linear theory (——) with the measured coherence at the spectral peak frequency f_m (⊙) plotted against kl ($= 2\pi l/L$) for (*a*) $U = 10\,\mathrm{m/s}$ and (*b*) $U = 15\,\mathrm{m/s}$. The angular distribution function is assumed as $S(\theta) \sim \cos^m\theta$, $m = 2, 4, 6$.

measured spectrum ($f/f_m \lesssim 3$). It will be shown later that the much larger increase in our measured phase velocity at $f/f_m \gtrsim 1{\cdot}8$, can be largely attributed to the effect of forced waves.

6. Comparison between theory and measurements

Effects of angular spreading

First, the effects of angular spreading of waves on the phase velocity and coherence are studied by comparing the measured results with the predictions of the theory. Since nonlinear effects are expected to be relatively small near the spectral peak frequency, phase velocity and coherence were calculated by using the cross-spectrum of linear free waves $Cr_1(\omega, 1)$. That is, theoretical calculations were done within a frame of linear theory. Figure 8 shows an example of the results, where the angular distribution function is assumed as $\cos^m\theta$, $m = 2$, 4, 6. The figure shows that the angular distribution function of the form $\cos^4\theta$ gives the best fit to the data both for C/C_0 and for the coherence near the spectral peak frequency ($f/f_m \cong 1$). Such a comparison was also made for the data of other cases: different spacings of wave gauges and different wind speeds. It was found that the linear theory can explain the

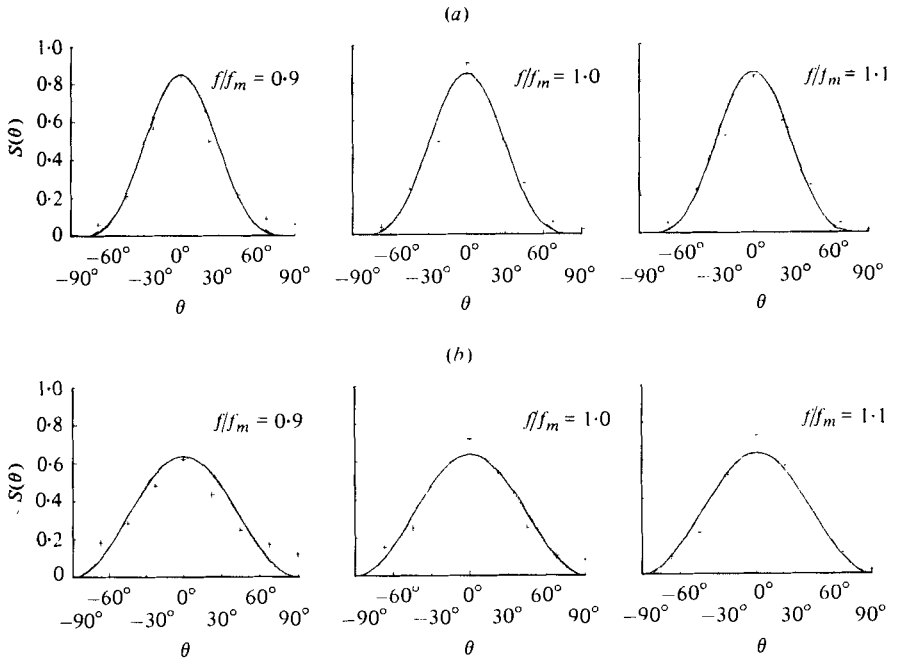

FIGURE 10. Examples of the measured angular distribution function, (+). ——, $S(\theta) \sim \cos^m \theta$. (*a*) $m = 4$ for $U = 10\,\mathrm{m/s}$, (*b*) $m = 2$ for $U = 15\,\mathrm{m/s}$.

measured data in the following frequency range: $f/f_m = 0{\cdot}8$ to $1{\cdot}6$ for $U = 10\,\mathrm{m/s}$, and $f/f_m = 0{\cdot}9$ to $1{\cdot}3$ for $U = 15\,\mathrm{m/s}$.

It was also found that the angular distribution function of the form $\cos^4\theta$ fits the data of the former case and that of the form $\cos^2\theta$ fits the data of the latter case. Figure 9 shows the relation between the coherence of the frequency components at the spectral peak and the separation distance of wave gauges. The distance l to the direction of wave propagation is normalized in the form kl, where $k = 2\pi/L$ is the wavenumber. The relations predicted by the linear theory are also shown in the same figure, where the angular distribution function was assumed again as $S'(m)\cos^m\theta$, $m = 2, 4, 6$. Figure 9 shows that the angular distribution function $\cos^4\theta$ fits the data for $U = 10\,\mathrm{m/s}$ and $\cos^2\theta$ fits the data for $U = 15\,\mathrm{m/s}$. Assumptions for the angular distribution functions were verified in figure 10 by comparing the idealized form (5.2) with the distributions measured directly by the technique of rotational linear array (Cummins 1959).

It should be noted, however, that at large separation distance of wave gauges ($kl > 5$) the power m changes gradually with the increase of the separation distance. Closer investigation of the original data of the coherence showed that such phenomena are related to the attenuation of spectral energy. With increasing distance between two wave gauges the attenuation of the wave energy near the spectral peak increases gradually. Slight but anomalous decrease of the coherence was found in a frequency range where the attenuation of the wave energy was considerable.

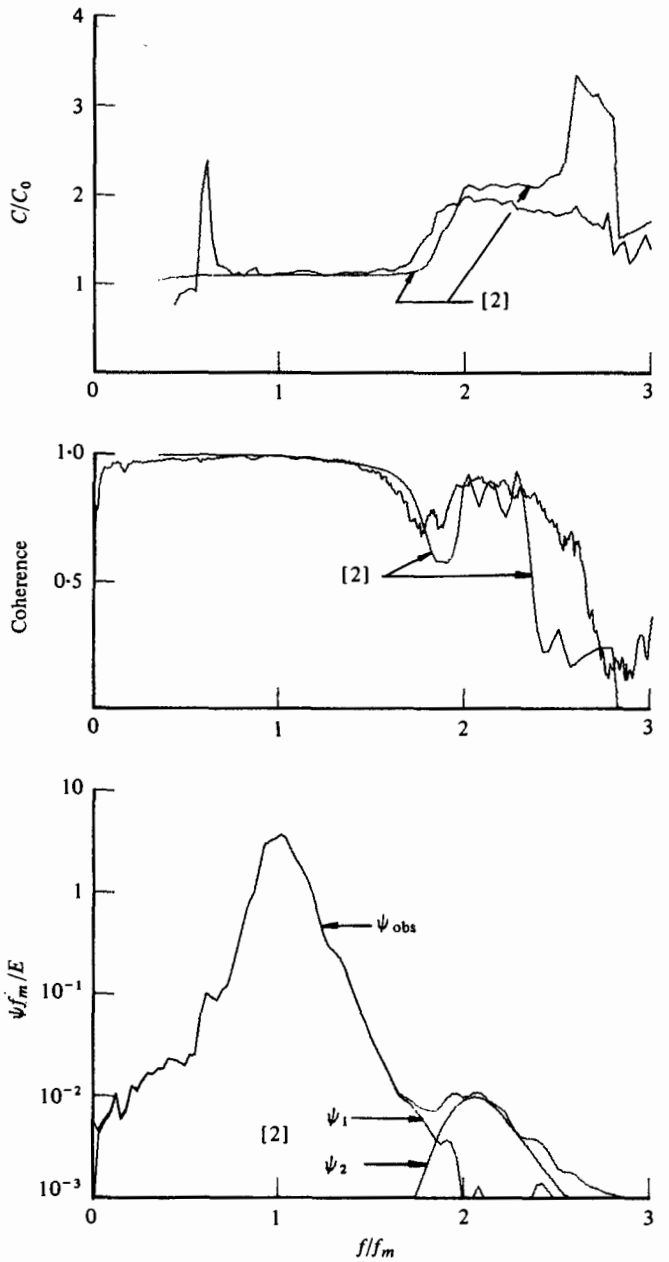

FIGURE 11. Comparison of the nonlinear theory with observational data. Normalized phase velocity C/C_0, coherence and normalized power spectra $\psi(f)f_m/E$ for $U = 10\,\mathrm{m/s}$ and $l = 4\,\mathrm{cm}$. Curve [2] is a second-order approximation to the nonlinear theory.

Nonlinear effects

Although the linear theory of two-dimensional random waves shows a fairly good agreement with our measurements, the validity is confined only to the dominant part of the wave spectrum near the spectral peak. That is, neither rapid increase of the phase velocity nor corresponding local decrease of the coherence can be explained by

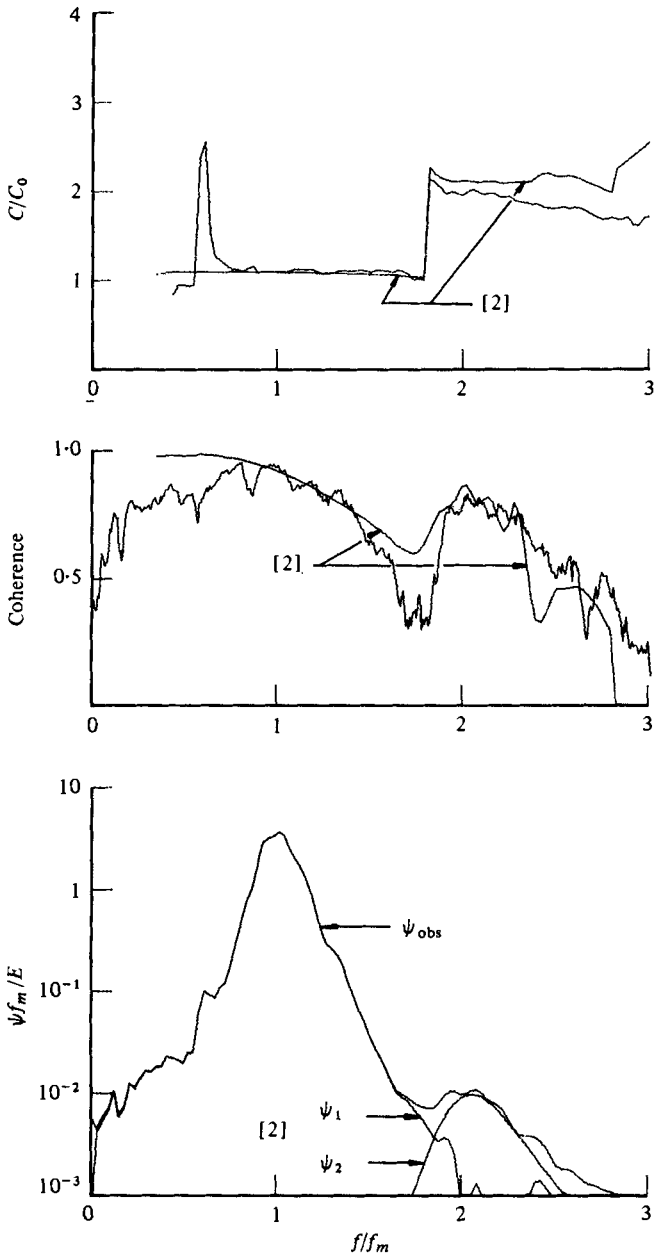

FIGURE 12. The same as figure 10 except for $U = 10\,\mathrm{m/s}$ and $l = 12\,\mathrm{cm}$.

the linear theory. Therefore, the results are compared, in the next step, with the nonlinear theory presented in I.

Figures 11–13 show the results of such comparisons. Each figure shows, from the top to the bottom, the normalized phase velocity C/C_0, the coherence, and the normalized power spectrum $\Psi f_m/E$ at the upward station, respectively, as the function of a dimensionless frequency f/f_m. Here, E is the total energy of the wave spectrum.

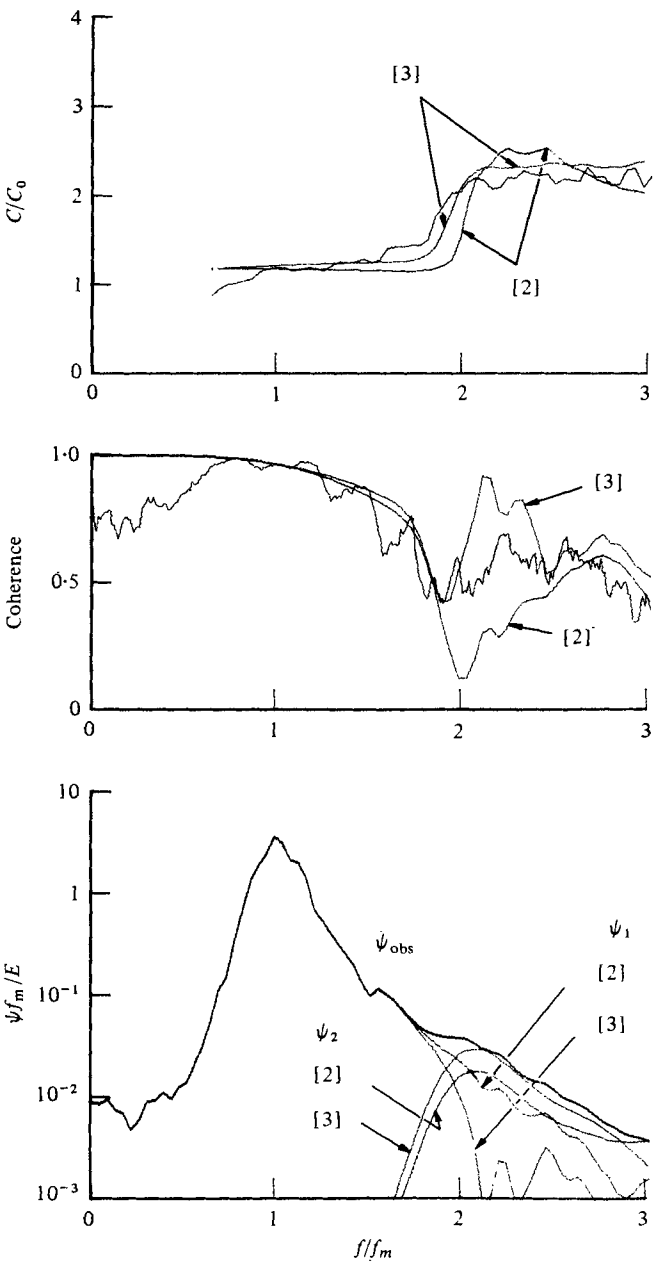

FIGURE 13. The same as figure 10 except for $U = 15\,\mathrm{m/s}$ and $l = 12\,\mathrm{cm}$. Curve [3] is a third-order approximation to the nonlinear theory.

In each figure, the curve [2] corresponds to the prediction of the second-order theory of two-dimensional random waves. The angular distribution function was assumed to be proportional to $\cos^4\theta$ for $U = 10\,\mathrm{m/s}$, and $\cos^2\theta$ for $U = 15\,\mathrm{m/s}$. These figures show an exceedingly good agreement between the nonlinear theory and the present measurements.

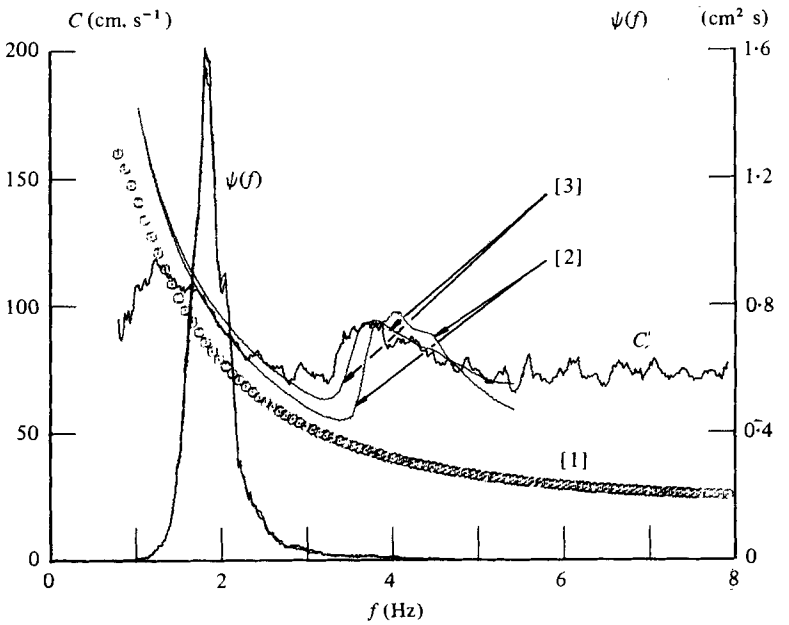

FIGURE 14. Power spectrum, and phase velocity (data are the same as those shown in figure 13). [1] is a one-dimensional linear theory, [2] and [3] are a second-order approximation and a third-order approximation respectively, to the two-dimensional nonlinear theory.

For the case of $U = 15\,\mathrm{m/s}$, two theoretical curves, the second-order approximation denoted by [2] and the third-order approximation denoted by [3], are compared with the measurements because the nonlinearity of the waves is larger in this case ($U = 15\,\mathrm{m/s}$) than in the other case ($U = 10\,\mathrm{m/s}$). As expected, the third-order approximation shows better agreement with the measurement.

From the results shown in figures 11–13 we can conclude that every results of our measurements can be explained by the nonlinear theory of two-dimensional random waves presented in I. Furthermore, it can be seen that the spectral energy near the frequency $f/f_m = 2$ can be largely attributed to the nonlinear effects. In other words, they are mostly due to the forced waves and not to the free waves. A very rapid increase of C/C_0 and a rapid local decrease of the coherence occur at the frequency where the spectral density of the free waves Ψ_1 coincides with that of the forced waves Ψ_2. It can be seen from comparison of figure 11 with figure 12 that the increase of C/C_0 near $f/f_m = 1{\cdot}8$ is very rapid for the latter case ($l = 12\,\mathrm{cm}$) as compared to the former case ($l = 4\,\mathrm{cm}$). Such a difference can be attributed to the effect of the spacing of the wave gauges. A simple calculation (see appendix) shows that the change in C/C_0 is relatively gradual for the case of narrow spacing of wave gauges but it becomes very rapid for the case of the wide spacing. When $kl = 2\pi$, the change of C/C_0 becomes discontinuous at $a = 1$.

It is also quite natural that the measured C/C_0 is approximately 2 for the frequency range $1{\cdot}8 < f/f_m < 3$, because the spectral components in this range are almost entirely due to the forced waves accompanied by the dominant waves in a frequency range $0{\cdot}9 < f/f_m < 1{\cdot}5$.

An example of the dimensional expression of the present results is shown in figure

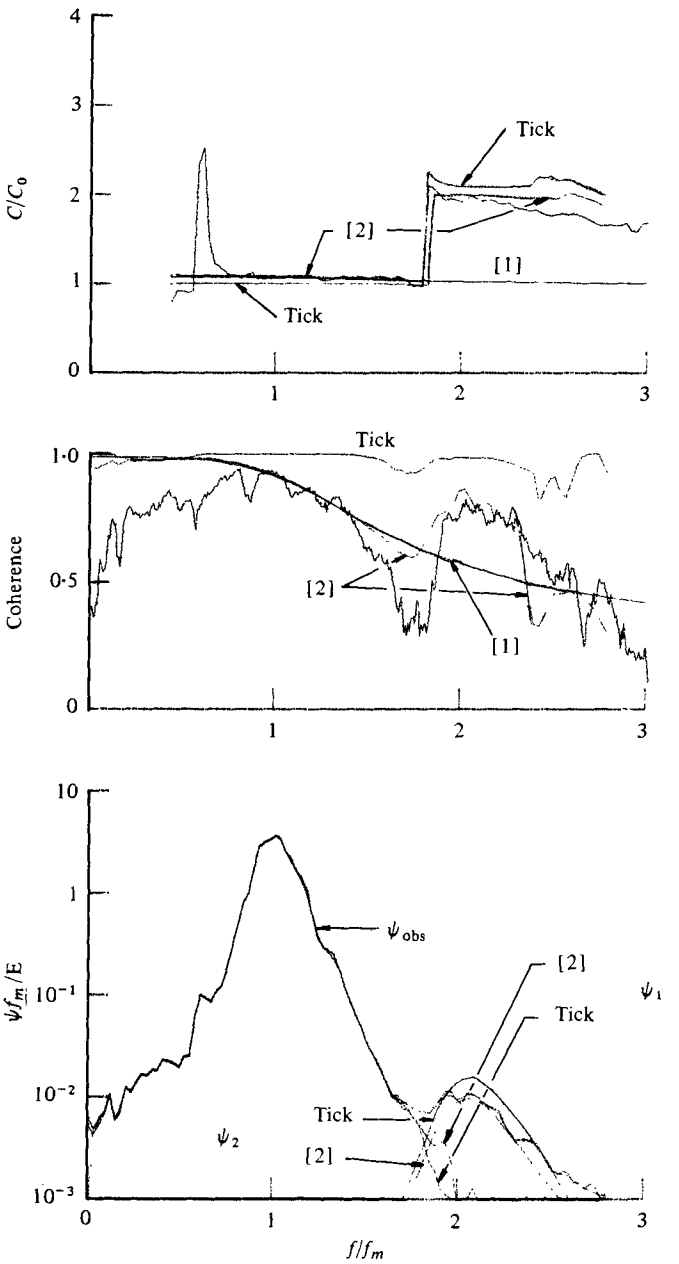

FIGURE 15. Comparison of the observational data with two-dimensional linear theory [1] and two nonlinear theories: two-dimensional theory [2] (Masuda *et al.* 1979); and one-dimensional theory (Tick 1959). The data are the same as in figure 11.

14 to compare our present results with those of the other investigators (Yefimov *et al.* 1972; Ramamonjiarisoa 1974). Here again we can see a satisfactory agreement between the nonlinear theory and the experiment in the decay area. Slight differences between our results and those of the other investigators can be attributed to the different spacing of wave gauges and the effect of drift current.

In order to determine the individual or combined effects of the various factors affecting the wave velocity, computations were done by using a linear model of two-dimensional waves (Yefimov *et al.* 1972), a nonlinear model of one-dimensional waves (Tick 1959) and our nonlinear model of two-dimensional waves (Masuda *et al.* 1979). The results of each computation are compared with our measurements in figure 15. As may be seen from the figure, a nonlinear model of two-dimensional waves shows the best fit to the data. Tick's model describes the behaviour of the phase velocity fairly well but fails to predict that of the coherence. The linear model can be applied only to the dominant part of the spectrum.

Some remarks should be added to these conclusions. The present experiment is confined to wind waves in the decay area. Therefore, it is quite natural that we need to consider the effects of the drift current in the analysis of the phase velocity of wind waves in the generation area. In fact, according to our preliminary analysis of the wave data in the generation area, the relative phase velocity C/C_0 changes gradually from $C/C_0 \doteqdot 1$ at $f/f_m = 1$ to $C/C_0 \doteqdot 2$ at $f/f_m = 2$. That is, the rapid change of C/C_0 near $f/f_m = 1{\cdot}8$ is not observed, which is mainly owing to the effects of the drift current. Furthermore, the ratio of the free wave components to the forced wave components may be different for wind waves in the generation area.

7. Conclusions

The conclusions of this study are summarized as follows. For wind waves in the decay area, the phase velocity and the coherence of the energy-containing components near the spectral peak are very close to those given by the linear theory. However, spectral energy in a high frequency region ($f > 1{\cdot}8f_m$) is largely due to the second-order (forced) waves and contributions of the free waves are relatively small. The rapid increase of the phase velocity and the rapid local decrease of the coherence occur at a frequency near $1{\cdot}8f_m$, both of which are due to the effects of the second-order (forced) waves coexisting with the free waves.

When we apply the present results to the analysis of wind waves in the generation area, we need to consider the effects of the drift current, since the present results are obtained by waves unaffected by the drift current.

The authors are indebted to Mr T. Honda, Mr K. Eto and Mr M. Tanaka for their assistance in the laboratory experiment, and to Miss N. Uraguchi and Miss M. Hojo for typing the manuscript. They also wish to express their appreciation to Dr H. Honji for his invaluable comments on the first draft of the paper.

Appendix

Let us consider the random wave field of the form

$$\eta(x,t) = A(\omega)\exp\left\{i\frac{\omega^2}{g}x - i\omega t\right\} + B(\omega)\exp\left\{i\frac{\omega^2}{2g}x - i\omega t\right\}, \tag{A 1}$$

where A and B are uncorrelated random amplitudes of free and forced waves respectively. The first term corresponds to one free wave and the second to the second

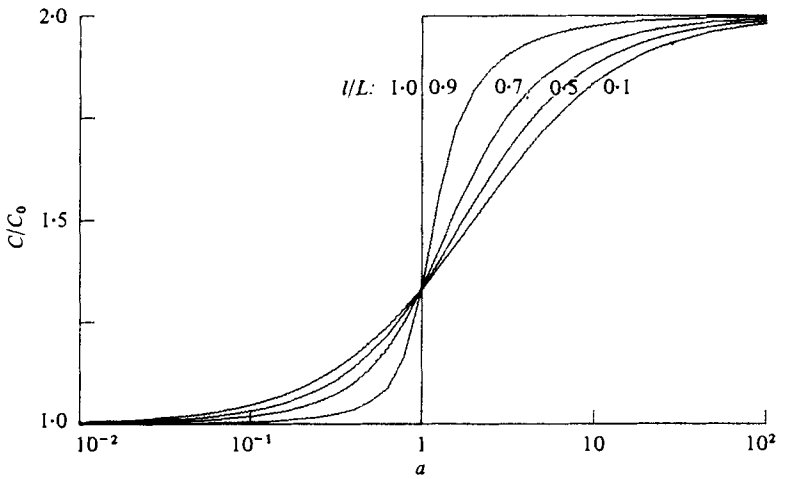

FIGURE 16. C/C_0 plotted against a for various l/L, where $a = \langle B^2\rangle/\langle A^2\rangle$ and $l/L = \omega^2 l/2\pi g$.

harmonic of the other free wave

$$A\left(\frac{\omega}{2}\right)\exp\left\{i\frac{1}{g}\left(\frac{\omega}{2}\right)^2 x - i\left(\frac{\omega}{2}\right)t\right\}, \tag{A 2}$$

which propagates twice as fast as the first free wave.

The phase velocity determined from the cross-spectrum of wave data $\eta(0,t)$ and $\eta(l,t)$, is given, in a normalized form, as

$$\frac{C}{C_0} = \frac{\omega^2}{g}\, l/\tan^{-1}\left\{\frac{\sin\omega^2 l/g + a\sin\omega^2 l/2g}{\cos\omega^2 l/g + a\cos\omega^2 l/2g}\right\}, \tag{A 3}$$

where a is the ratio of the forced wave energy $\langle B^2\rangle$ to the free wave energy $\langle A^2\rangle$ at fixed ω, and $C_0 = g/\omega$.

The relation between C/C_0 and a, which is given by (A 3), is shown in figure 16, where a relative spacing l/L ($= \omega^2 l/2\pi g$) is taken as a parameter. Figure 16 shows that C/C_0 is very close to unity if the free wave energy is much larger than the forced wave energy, i.e. $a \ll 1$, whereas in the opposite case, $a \gg 1$, C/C_0 becomes very close to two. Moreover, C/C_0 increases very rapidly near $a = 1$ and the increasing rate is larger for the case of larger spacing of the wave gauges.

REFERENCES

BARRICK, D. E. & WEBER, B. L. 1977 On the nonlinear theory for gravity waves on the ocean's surface. Part II. Interpretation and applications. *J. Phys. Oceanog.* **7**, 11–21.

CUMMINS, W. E. 1959 The determination of directional wave spectra in the TMB maneuvering–seakeeping basin. *Navy Dept. David Taylor Model Basin Rep.* 1362.

HASSELMANN, K. 1962 On the nonlinear energy transfer in a gravity-wave spectrum. Part 1. General theory. *J. Fluid Mech.* **12**, 481–500.

HUANG, N. E. & TUNG, C. 1976 The dispersion relation for a nonlinear random gravity wave field. *J. Fluid Mech.* **75**, 337–345.

HUANG, N. E. & TUNG, C. 1977 The influence of the directional energy distribution on the nonlinear dispersion relation in a random gravity wave field. *J. Phys. Oceanog.* **7**, 403–414.

KATO, H. 1974 Calculation of the wave speed for a logarithmic drift current. *Rep. Port and Harbour Res. Inst.* **13**, 3–32.

LONGUET-HIGGINS, M. S. & PHILLIPS, O. M. 1962 Phase velocity effects in tertiary wave interactions. *J. Fluid Mech.* **12**, 333–336.

MASUDA, A., KUO, Y.-Y. & MITSUYASU, H. 1979 On the dispersion relation of random gravity waves. Part 1. Theoretical framework. *J. Fluid Mech.* **92**, 717–730.

PHILLIPS, O. M. 1960 On the dynamics of unsteady gravity waves of finite amplitude. Part 1. The elementary interactions. *J. Fluid Mech.* **9**, 193–217.

RAMAMONJIARISOA, A. 1974 Contribution à l'étude de la structure statistique et des mécanismes de génération des vagues de vent, Ph.D. thèse, l'Université de Provence, Institute de Mécanique Statistique de la Turbulence.

SHEMDIN, O. H. 1972 Wind-generated current and phase speed of wind waves. *J. Phys. Oceanog.* **2**, 411–419.

TICK, L. J. 1959 A nonlinear random model of gravity waves. I. *J. Math. Mech.* **8**, 643–651.

WEBER, B. L. & BARRICK, D. E. 1977 On the nonlinear theory for gravity waves on the ocean's surface. Part I. Derivations. *J. Phys. Oceanog.* **7**, 3–10.

YEFIMOV, V. V., SOLOV'YEV, YU. P. & KHRISTOFOROV, G. N. 1972 Observational determination of the phase velocities of spectral components of wind waves. *Isv. Atmos. Oceanic Phys.* **8**, 435–446.